Assessing Satellite-derived Inter-annually Varying Snow/Firn Density Estimates Over the Greenland Ice Sheet during 2003-2009

Xiaoli Su[1,2*], C.K. Shum[3,5], Kenneth C Jezek[3,4], Junyi Guo[3], Ian Howat[3,4], Chungyen Kuo[6], and Zhicai Luo[1,2]

[1]The MOE Key Laboratory of Fundamental Physical Quantities Measurement and Hubei Key Laboratory of Gravitation and Quantum Physics, PGMF and School of Physics, Huazhong University of Science and Technology, Wuhan 430074, China, xlsu@hust.edu.cn, zcluo@hust.edu.cn

[2]Institute of Geophysics and PGMF, Huazhong University of Science and Technology, Wuhan 430074, China

[3]Division of Geodetic Science, School of Earth Sciences, The Ohio State University, Columbus, OH 43210-1398, USA, ckshum@osu.edu, jezek.1@osu.edu, guo.81@osu.edu, howat.4@osu.edu

[4] Byrd Polar and Climate Research Center, The Ohio State University, Columbus, OH 43210-1398, USA

[5] Institute of Geodesy and Geophysics, Chinese Academy of Sciences, Wuhan 430077, China

[6]Department of Geomatics, National Cheng Kung University, Tainan 701, Taiwan, kuo70@mail.ncku.edu.tw

Corresponding author: Xiaoli Su (xlsu@hust.edu.cn)

Key Points:

- We jointly analyze inter-annual anomaly of mass change and refined elevation change by repeat-track analysis over the Greenland ice sheet
- Inter-annually varying snow/firn density is relatively larger over Western Greenland, compared to other regions in the Greenland ice sheet
- Satellite-derived density is validated with in situ data for the first time mostly along the central ice divide

Abstract

Knowledge of snow/firn density is important for deriving ice sheet mass change from satellite altimetry and for surface mass balance modeling. However, snow/firn densities are largely unknown over the Greenland ice sheet (GrIS) away from isolated direct measurements in boreholes. Density assumptions are widely used when converting volume change from satellite altimetry into mass change, which could introduce errors. Here we extract the inter-annual anomalies of mass change from Gravity Recovery And Climate Experiment (GRACE) data and the refined ice elevation change through the repeat-track analysis of Environmental Satellite (Envisat) altimetry data retrieved using both the ICE1 and ICE2 waveform retracking algorithms. By combining these two types of inter-annual anomalies (GRACE+ICE1 and GRACE+ICE2), we investigate the inter-annually changing snow/firn density estimates over the GrIS during the 2003–2009 period. Our results demonstrate that satellite-derived density is relatively greater over Western GrIS, with magnitude falling between 300 kg/m^3 and 917 kg/m^3 occupying more than 71% of the GrIS. At the regional scale, GRACE+ICE1 derived density agrees well with that from density profiles of 9 ice cores at Summit Station, Central GrIS, with relative errors less than 5%. Satellite-derived densities are further compared with that from 110 ice cores mostly along the central ice divide. The percentage of GRACE+ICE1 derived densities with relative errors less than 20% exceeds 84%, as opposed to 41% for GRACE+ICE2. Satellite-derived densities could possibly underestimate the inter-annually varying snow/firn density over Southern GrIS. This study may provide constraints on the currently applied density assumptions for the GrIS.

Plain Language Summary

Snow/firn density is a key variable for us to understand the mass balance of the Greenland ice sheet (GrIS) using satellite altimetry. It can be obtained by making isolated direct measurements in boreholes. However, it is rather costly and difficult to perform such measurements everywhere. In this study, we perform a joint analysis of mass change from GRACE and elevation change from Envisat at the inter-annual timescale, aiming at deriving and validating inter-annually varying snow/firn density estimates over the GrIS. We found that satellite-derived density values are relatively large in Western GrIS, with potential underestimates occurred in Southern GrIS. Satellite-derived densities agree with those from in situ measurements mostly along the central ice divide. This work may provide constrains on the currently applied density assumptions and contribute to improving snow/firn models for the GrIS.

1 Introduction

Satellite altimetry provides substantial repeat measurements about elevation change of the Greenland ice sheet (GrIS), which enable us to estimate the related volume change (Zwally et al., 1989; Bamber, 1994; Krabill et al., 1995; Sorensen et al., 2015; Nilsson et al., 2016). To infer mass change of the GrIS from the volume change or evaluate the contribution from the GrIS to sea level rise using satellite altimetry, the density associated with the corresponding volume change is required (Arthern and Wingham, 1998; Thomas et al., 2001). However, such densities can vary with time, snow depth and changing climatic conditions, which prevents satellite altimetry from accurately deriving mass change from the observed volume change (Howat et al., 2008; Kuipers Munneke et al., 2015). In order to investigate the GrIS mass balance using satellite altimetry data, different empirical density assumptions or density values based on firn compaction models are commonly applied to convert the observed volume change into mass change. As listed in Table 1, density values of 400 kg/m^3 and 900 kg/m^3 may be applied

separately for deriving mass changes of upper firn layers and ice dynamical components from their corresponding volume changes (Zwally et al., 2005; Shepherd et al., 2012); elevation-based assumptions are also used by the satellite altimetry community, i.e., 600±300 kg/m^3 for regions with elevation above 2000 m and 900 kg/m^3 for regions below 2000 m; other approaches, such as applying density models and empirical relations, can be also found in Sorensen et al. (2011), Bolch et al. (2013) and McMillan et al. (2016). Different density assumptions will cause discrepancies among the derived mass change of the GrIS, even if the same volume change is obtained from satellite altimetry. As pointed out by Shepherd et al. (2012), the greatest uncertainty of deriving ice sheet mass change using satellite altimetry can be attributed to the inaccuracy of the density of snow/firn associated with the volume change. Consequently, the snow/firn density associated with the measured volume change is crucial for accurately estimating the mass balance of the GrIS via satellite altimetry.

Table 1 Density assumptions used for the GrIS in previous studies. The following abbreviations are used: ERS-1/2 – European Remote-sensing Satellite-1/2; ATM – Airborne Topographic Mapper; ICESat – the Ice, Cloud, and land Elevation Satellite; Envisat – Environmental Satellite; CryoSat-2 – the Cryosphere Satellite-2.

Previous studies	Mission	Time period	Density [kg/m^3]
Zwally et al. (2005)	ERS-1/2	1992/04 – 2002/10	400; 900
Thomas et al. (2006)	ATM/ICESat	1998/09 – 2004	600; 900
Slobbe et al. (2009)	ICESat	2003/02 – 2007/04	600; 900
Sorensen et al. (2011)	ICESat	2003/10 – 2008/03	density model
Shepherd et al. (2012)	ERS-1/2, Envisat	1992/05 – 2010/09	400; 900
Bolch et al. (2013)	ICESat	2003/10 – 2008/03	empirical relation
McMillan et al. (2016)	CryoSat-2	2011/01 – 2014/12	Firn densification model

Another geodetic technology, namely the Gravity Recovery And Climate Experiment (GRACE) gravimetry, provided the Earth's global temporal gravity field observations, which made it possible to infer monthly mass redistributions on and below the Earth's surface with a relatively coarse spatial resolution of ~333 km since March 2002 (Tapley et al., 2004). Nevertheless, GRACE-derived mass trends are prone to uncertainties in the glacial isostatic adjustment (GIA) models**,** especially over ice sheets (Guo et al., 2012) at the regional scale (Sutterley et al., 2014). GRACE-derived mass trends are also susceptible to be influenced by inter-annual variations of mass change (Sasgen et al., 2012). Over the GrIS, the inter-annual components of mass change are significant, with magnitude larger than 100 Gt/yr (Bamber et al., 2018). The length of the current data records is relatively short (Wouters et al., 2013), so it is impossible to fully distinguish the mass trend from the inter-annual mass variations. Besides, the GRACE mission ended its science tasks in October 2017, and the Gravity Recovery And Climate Experiment Follow-On (GRACE-FO) is resuming data collection after its successful launch on 22nd May 2018. However, there is a data gap for mass changes measured by gravimetry over the GrIS. Satellite altimetry can fill that gap provided that the estimates of snow/firn density over the GrIS are robust to convert altimetry to mass changes.

Currently, it is not feasible to investigate the snow/firn density over the entire GrIS purely using in situ data, which are quite limited in terms of the number of measurements and the spatial distribution (Montgomery et al., 2018). Furthermore, the density obtained from in situ data cannot be directly applied to convert volume change obtained from satellite altimetry into mass change. On the one hand, the snow/firn density is a function of variables including time,

position and climatic conditions. On the other hand, over regions with ice dynamics, satellite altimetry derived volume change includes surface mass balance and ice dynamical change (Kuipers Munneke et al., 2015). If only the upper snow/firn densities are used over these regions, one could underestimate the true mass change from volume change. Snow/firn densities based on firn densification models or regional climate models can be used but they are limited by uncertainties in the forcing datasets (Fettweis et al., 2017), by the surface snow model parametrizations (Fausto et al., 2018), and by the inaccurate model formulation (Steger et al., 2017; Noel et al., 2018).

The combination of GRACE gravimetry and satellite altimetry provides an opportunity to constrain the density of snow/firn over the GrIS. In the study of Su et al. (2015), the authors generally found high correlations between inter-annual variations of mass change from GRACE and elevation change from Envisat altimetry over the GrIS. Based on the assumption that GRACE and Envisat detected the same geophysical signals at the inter-annual scale, they estimated the nominal densities of snow/firn at 9 regions by combining GRACE gravimetry and Envisat altimetry, with a focus on obtaining high spatial resolution inter-annual mass variations based on density-corrected altimetry data. By nominal density, we mean the density value computed by taking the GRACE-derived mass change and dividing by the volume change from Envisat altimetry, after detrending both time series and removing seasonal variations. Although the possibility to constrain the snow/firn density purely by using geodetic measurements was proposed previously (Wahr et al., 2000), the nominal densities are scarcely estimated over the entire GrIS. More importantly, no validation has been performed to examine satellite-derived nominal density.

In this study, we analyzed Envisat mission radar altimetry data using the improved repeat-track analysis combined with updated GRACE data processing, aiming at accurately retrieval of satellite-derived nominal densities at inter-annual temporal scale over the entire GrIS, followed by a validation of satellite-derived nominal density values using in situ data (110 ice cores). GRACE data from Center for Space Research (CSR) at the University of Texas (Austin), Deutsches GeoForschungsZentrum (GFZ) German Research Centre for Geosciences and the Jet Propulsion Laboratory (JPL) at the California Institute of Technology are analyzed separately together with Envisat data retrieved by two different radar waveform retracking algorithms at the inter-annual timescale. We evaluate the sensitivity of satellite-derived density values to the algorithm used to retrieve Envisat data. Also, the impact of the accuracy of GRACE-derived inter-annual anomalies on our results is assessed. Finally, satellite-derived densities are validated with in situ data for the first time. This study suggests the potential constraints from geodetic observations on the density of snow/firn inter-annually changing over the GrIS.

2 Data and Methods

2.1 GRACE data analysis

We selected coincident Envisat and GRACE data during the period from January 2003 to December 2009. Considering the accuracy of GRACE-derived inter-annual anomalies, we analyze GRACE Level 2 Release-6 (RL06) monthly gravity field solutions separately from CSR (Bettadpur, 2018), GFZ (Dahle et al., 2018) and JPL (Yuan, 2018). Each GRACE monthly gravity solution consists of spherical harmonic coefficients (spherical harmonic series in spherical coordinates used to express geopotential) with degree and order complete to 60.

Coefficients $C_{2,0}$ are replaced by $C_{2,0}$ estimates from satellite laser ranging (Cheng and Tapley, 2004), and coefficients of degree one derived using the method of Swenson et al. (2008) and Sun et al. (2016) are added to correct for the geocenter motion. To remove the spurious north-south stripes in mass change derived from GRACE monthly gravity solutions, Gaussian smoothing with a radius of 300 km is applied. Gaussian smoothing will cause signals on land to leak into coastal ocean. To correct for signal leakage caused by Gaussian smoothing, leakage reduction is conducted using the approach of Guo et al. (2010). After generating time series of mass change at each regular grid cell, the time series can be decomposed into an offset, a linear trend and seasonal components through fitting based on least squares. Here the decomposition can be written like the following:

$$\mathrm{m}(t_k) = a_0 + a_1 t_k + a_2 \sin\left(\frac{2\pi}{T_1} t_k\right) + a_3 \cos\left(\frac{2\pi}{T_1} t_k\right) + a_4 \sin\left(\frac{2\pi}{T_2} t_k\right) + a_5 \cos\left(\frac{2\pi}{T_2} t_k\right) \quad (1)$$

in which, $\mathrm{m}(t_k)$ is mass variation in equivalent water height (EWH), t_k is time in year relative to year 2003 for the k^{th} observation, T_1 and T_2 correspond to periods of a year and half a year, and $a_0, \cdots, a_5$ are unknown parameters.

By removing the linear trend and seasonal components from the mass change time series, the inter-annual anomalies can be obtained by applying a moving average with a one year long window to the residuals to further remove the remnant seasonal variations. Glacial isostatic adjustment signal is removed, as it is a part of linear components of mass change. Additional information of GRACE data processing over the GrIS can be obtained from Groh et al. (2019).

2.2 Envisat data post-processing

The 18-Hz Envisat Geophysical Data Record (GDR) product (version 2.1) during the period from January 2003 until December 2009 are processed over the GrIS using a modified repeat-track analysis. We select this study period, mostly considering that the quality of Envisat data during the mission commissioning phase (March 2002~December 2002) may not be good enough and the repeat track analysis requires measurements obtained by satellite operated in a repeat-orbit phase. The modified repeat-track analysis does not require auxiliary data such as a digital elevation model to remove the effects of surface slope. It directly uses the accumulated Envisat altimetry profiles to correct the surface slope, which avoids the contribution of potential inaccuracies in the auxiliary data (Su et al., 2016). As Envisat-observed elevation can be separately retrieved by two algorithms, namely the ICE1 and the ICE2 algorithms, elevation change time series are generated using each algorithm in order to evaluate the potential impact from the algorithm used to retrieve Envisat data on satellite-derived density. To be noted, the ICE1 algorithm is based on the offset center of gravity echo model (Wingham et al., 1986), while the ICE2 algorithm is optimized for ocean-like echoes reflected from the ice sheet surface (Legresy and Remy, 1997). After generating elevation change time series, we compare the total number of valid data points obtained separately from both algorithms (Table S1), the Root Mean Square (RMS) of the corresponding elevation change time series (Figure S1 and Table S1), and the uncertainties of the corresponding linear trends (Figure S2 and Table S1). It can be seen that the performance of these two algorithms on retrieving elevation change is similar, with slight differences shown on the three statistical quantities.

In a manner similar to what was done for mass change, the inter-annual elevation change time series can be calculated by subtracting an offset, a linear trend and seasonal components, obtained by fitting elevation change time series. By interpolating at the exact epoch of GRACE

data and applying a moving average with one year long window, the inter-annual time series can be formed at each nominal track and then averaged to the same regular grids as we use for GRACE data. To be commensurate with GRACE data, we apply the same Gaussian smoothing with a radius of 300 km to Envisat data. We also perform signal leakage reduction to avoid signal leaking into region with rugged terrain or without data coverage.

2.3 Surface mass balance (SMB) estimate

To test that GRACE gravimetry and Envisat altimetry can detect the same geophysical process at the inter-annual scale, we use monthly SMB estimates (covering January 2003 to December 2009) outputted by the regional climate model RACMO2/GR (van den Broeke et al., 2009). The RACMO2/GR model can capture temporal behavior of the SMB variations, and its uncertainty can be considerably reduced by generating cumulative SMB variations with respect to the reference period 1961-1990 (Sasgen et al., 2012). We calculate monthly cumulative SMB variations during the study period 2003-2009 at the same regular grids as we use for GRACE data. To be commensurate with GRACE data, we apply the same Gaussian smoothing with a radius of 300 km to the monthly cumulative SMB anomalies and further perform the same signal leakage correction. Finally, the inter-annual SMB anomalies are extracted from the monthly cumulative SMB variations by using the same approach as done for GRACE data.

2.4 In situ data analysis

Two kinds of in situ data are utilized in this study. These are the density profiles of snow pits and ice cores from the SUMup dataset provided by the surface mass balance and snow on sea ice working group (Montgomery et al., 2018). The former was obtained at the Summit Station, Central Greenland at a nominal monthly interval. It covers the time period from August 2003 to December 2009. There are totally 75 density profiles available. Each snow pit was sampled to 99-cm depth, at a resolution of 3 cm along the vertical direction. The latter includes 110 density profiles of ice cores which were mostly sampled along the central ice divides during the 1955-2009 period.

Satellite-derived density is the density of snow/firn/ice changing at the inter-annual timescale, the density profiles from the in situ data cannot be directly applied to conduct the validation, as the seasonally changing firn layers in the in situ data should be excluded. We first use the density profiles of snow pits to search for seasonally changing firn layers. We then apply the density profiles of ice cores after excluding the seasonally changing density of snow/firn to perform the validation. Here we adopted a quasi-"Eulerian" approach to approximately search for seasonally changing snow/firn layers (Alley et al., 1993). It first finds the measured depth where water equivalent depth equals 25 cm approximating a year of snow accumulation. Time series of annual layer thickness (depth from surface to 25 cm water equivalence) can be then obtained (Dibb and Fahnestock, 2004). By computing average density for arbitrary depth intervals in the series of pits, anti-correlations can be found between most of them and variations in annual layer thickness. Figure S3 depicts the correlation between annual layer thickness and average density variations in different depth range (0-99 cm, 3-99 cm, ⋯, and 96-99 cm), and the corresponding p-value. It is apparent that anti-correlations reduce gradually as the depth increases, with most of p-values less than 0.05. At a confidence level of 95%, no significant correlation can be found between average density variations in the 90 to 99 cm, 93 to 99 cm, 96 to 99 cm depth range and variations in annual layer thickness, respectively. This may suggest that seasonal variations

associated with compaction in the top "year" of the snowpack mainly occur from the surface to the depth of 90 cm. That is, inter-annual variations of snow/firn mostly occur below the upper meter layers (Graeter et al., 2017). According to Figure 1 by Bader (1953) at Eismitte (71.75°N, 40.75°W), the variations of snow/firn layers corresponding to the observation time of 7 years (the geodetic observation time) should mainly concentrate on the snow/firn layers about 5 m below the ice sheet surface. Considering the difference on accumulation along the central ice divide (Bolzan and Strobel, 1994), we select average density of snow/firn with depth ranging below the seasonally changing layer to 4 m to examine satellite-derived density. To be noted, the depth range is only fixed for 9 ice cores at the Summit Station, Central GrIS. As to the other 101 ice cores, the depth used to calculate average density from single ice core is determined according to the mean of annual accumulation provided by the RACMO2/GR model, as shown in Figure S4.

2.5 Estimating the inter-annually changing density of snow/firn over the GrIS

Given that GRACE gravimetry and Envisat altimetry can sense the same geophysical process at the inter-annual scale and the firn compaction associated with air temperature at the inter-annual timescale is small and negligible (Zwally and Li, 2002), the inter-annually changing density of snow/firn the GrIS can be estimated by linear regression, which can be written as the following:

$$\rho_w h_w^k = \rho_E h_E^k + b \tag{2}$$

where $\rho_w = 1000\,\mathrm{kg/m^3}$, h_w^k is the inter-annual mass change in EWH(cm) from GRACE data during the k^{th} ($k = 1, 2, \cdots \mathrm{N}$) observation time, h_E^k is the inter-annual elevation change (cm) measured by Envisat during the same epoch, N is the total number of observations during the study period. ρ_E is satellite-derived inter-annually changing density, and b is the potential bias between these two inter-annual mass changes separately observed by GRACE and Envisat.

To be mentioned, there could be special cases about satellite-derived density over regions with complicated geophysical processes, i.e., both snow accumulation and ice dynamics (Li and Zwally, 2011). Over such regions, assuming the inter-annual elevation change caused by snow accumulation and ice dynamics can be separately marked by h_{Es}^k and h_{Ei}^k, then we can have:

$$\rho_E h_E^k = \rho_s h_{Es}^k + \rho_i h_{Ei}^k \rightarrow \rho_E = \rho_s + (\rho_i - \rho_s)\frac{h_{Ei}^k}{h_{Ei}^k + h_{Es}^k} \tag{3}$$

where ρ_i is the pure ice density, and ρ_s is the density of snow. As snow accumulation will add surface elevation while ice dynamics reduces surface elevation, thus h_{Es}^k is positive and h_{Ei}^k is negative. Apparently, if $h_{Ei}^k + h_{Es}^k$ is positive, ρ_E is then less than ρ_s. That is, satellite data may underestimate the density over regions with both snow accumulation and ice dynamics.

3 Results, or a descriptive heading about the results

3.1 Similarity in the inter-annual anomalies from GRACE gravimetry, Envisat altimetry and SMB

Following the methods in section 2, we extract inter-annual anomalies of mass change from GRACE, elevation change from Envisat altimetry, and surface mass variation from SMB

over the GrIS during years 2003-2009 (See the animations in the supplementary material). From the animation, similar spatiotemporal characteristics can be found among these three inter-annual anomalies. To quantify the similarity among these inter-annual anomalies, the correlations between GRACE-derived inter-annual mass anomalies and Envisat-observed inter-annual elevation anomalies are firstly computed, as depicted by Figure 1. The top panel shows the cases where GRACE is compared with ICE1. High positive correlations (> 0.6) can be found over most regions, occupying 77%, 79% and 81% of the GrIS separately for Figure 1a, 1b and 1c. Weakly positive correlations can be found in parts of Northwest, North Central and Southeast GrIS. Negative correlations are only seen in a small region (less than 1% of the GrIS) in the North Central GrIS. For the cases where ICE2 is compared with GRACE (bottom panel in Figure 1), the percentage of regions with high positive correlations (>0.6) exceeds 90% of the GrIS. Weakly positive correlations can be seen in parts of North Central and Southeast GrIS. No negative correlations are found in Figure 1d, 1e) and 1f. By comparing the correlations for the ICE1 and ICE2 cases (i.e. Figure 1a with 1d, 1b with 1e and 1c with 1f), slight differences in the correlations can be seen, particularly over the Northwest and Southwest GrIS. This illustrates that consistent inter-annual mass anomalies are revealed over most regions in the GrIS by solutions from CSR, GFZ and JPL, while slight differences exist on the inter-annual elevation anomalies retrieved separately by the ICE1 and ICE2 algorithms. Compared to Figure 2 of Su et al. (2015), the total area where negative correlations occur is reduced from 7% to less than 1% of the GrIS, and no negative correlation is found over the Southeast GrIS. We think the improvement on correlations between inter-annual mass anomalies from GRACE and elevation anomalies from Envisat can be mainly attribute to the improved repeat-track analysis for removing topographic effect.

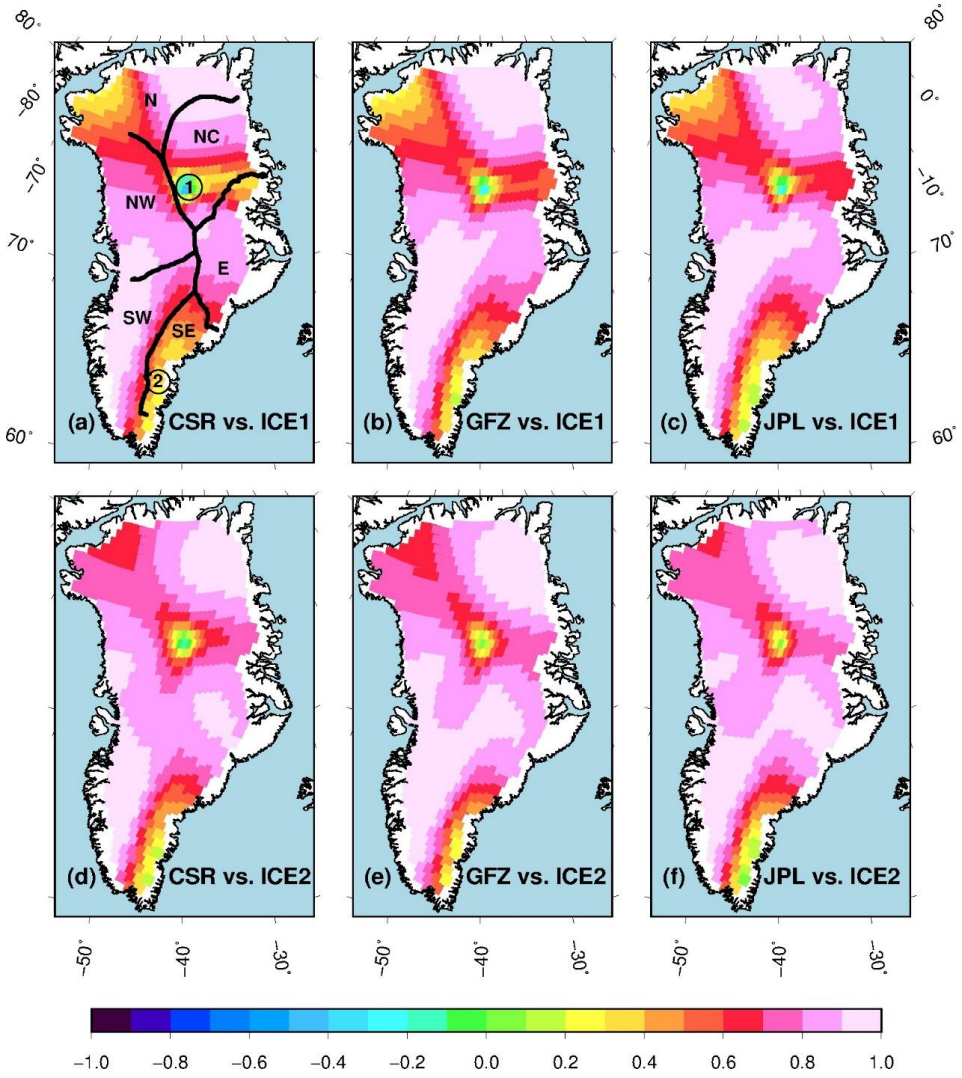

Figure 1 Correlations between inter-annual anomalies of mass change and elevation change during 2003-2009 for (a) CSR-published GRACE solutions and Envisat retrieved by the ICE1 algorithm, abbreviating as CSR vs. ICE1, (b) GFZ vs. ICE1, (c) JPL vs. ICE1, (d) CSR vs. ICE2, (e) GFZ vs. ICE2 and (f) JPL vs. ICE2. The central ice divide is depicted by the black line in bold in Fig. 1a, with N indicating North GrIS, NC for North Central GrIS, E for East GrIS, SE for South GrIS, SW for Southwest GrIS, and NW for Northwest GrIS.

We then compute the correlations between inter-annual anomalies from GRACE data and SMB over the GrIS, as shown by Figure 2. Inter-annual mass anomalies separately from CSR, GFZ and JPL published GRACE gravity solutions are used, with the corresponding correlation map marked as Figure 2a, 2b and 2c. For each subplot, high positive correlations can also be seen over most regions in the GrIS except for a small part of the North Central and Southeast GrIS. Together with correlations shown in Figure 1, high positive correlations in Figure 2 suggest that GRACE gravimetry and Envisat altimetry measure surface mass variations at the inter-annual time scale over most regions in the GrIS. Besides, the agreement of Figures 1 and 2 in terms of low correlation indicates that Envisat altimetry observations are still in agreement with SMB at regions where low correlations occur. Considering that SMB is an independent data source and GRACE-derived mass change include both SMB and mass change through ice

dynamics, we think the low correlations may be associated with ice dynamics occurring at the inter-annual time scale, as long as these three inter-annual signals are incredible. It is possible that a decrease in mass from GRACE is accompanied by mass loss through ice dynamics and high accumulation which leads to an increase in surface elevation (Li and Zwally, 2011). This will be discussed in further detail in the Discussion section. In addition, our result can increase the confidence in the GRACE and Envisat data analysis and the retrieval of SMB outputted by the RACMO2/GR model.

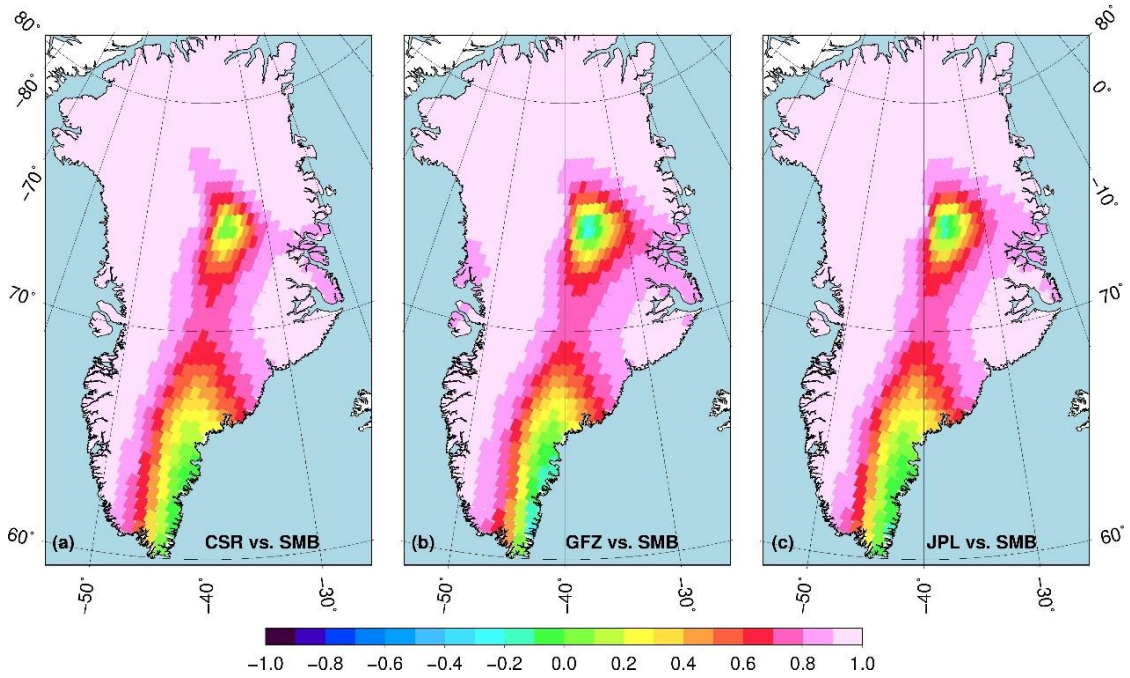

Figure 2 Correlations between GRACE-derived inter-annual mass anomalies and SMB-captured inter-annual surface mass anomalies during years 2003-2009. To be noted, CSR, GFZ and JPL published GRACE gravity solutions are separately analyzed, with the corresponding correlation map remarked as subplot (a) CSR vs. SMB, (b) GFZ vs. SMB and (c) JPL vs. SMB.

3.2 The nominal density map of snow/firn inter-annually changing over the GrIS

To further quantify the compatibility of the amplitudes of these inter-annual anomalies from GRACE gravimetry and Envisat altimetry over the GrIS, we attempt to estimate the inter-annually changing nominal density of snow/firn at each regular grid using the method mentioned in Section 2.5. As depicted by Figure 3, nominal densities are separately obtained over the GrIS by combining one of the three inter-annual mass anomalies derived from CSR, GFZ and JPL published gravity solutions and ICE1/ICE2-retrieved inter-annual elevation anomalies. For each subplot, nominal densities larger than 500 kg/m^3 can be seen over Northwest GrIS. Density values are quite small or physically unrealistic over regions with weakly positive and negative correlations. The percentages of nominal densities falling between 300 kg/m^3 and 917 kg/m^3 are 71%, 72% and 74% separately for cases where GRACE is combined with ICE1 (i.e., Figure 3a, 3b and 3c), as opposed to 82%, 84% and 82% for cases where GRACE is combined with ICE2 (i.e., Figure 3d, 3e and 3f). No nominal density value larger than 917 kg/m^3 is found in all the cases in Figure 3. Nominal density values of less than 0 kg/m^3 are found at regions with negative correlations, with a percentage of less than 1%. For cases where GRACE is combined

with ICE1 (the top panel in Figure 3), nominal densities are relatively smaller over Northwest and East GrIS, compared with those shown in cases where GRACE is combined with ICE2 (the bottom panel in Figure 3). Nominal densities are relatively larger over most of the region with latitude larger than 80ºN in the top panel, as opposed to those in the bottom panel. The differences between nominal densities for the combinations of different GRACE and altimetry products can be attributed to two issues. One is the algorithm used to retrieve Envisat data, and the other one is the analyzed GRACE gravity solutions. To better illustrate the impact on the nominal densities from the former, nominal density difference can be calculated in three cases like the following.

Case 1: nominal densities in Figure 3d subtracting those in Figure 3a

Case 2: nominal densities in Figure 3e subtracting those in Figure 3b

Case 3: nominal densities in Figure 3f subtracting those in Figure 3c

The nominal density differences corresponding to Case 1, 2 and 3 can be separately seen in Figure 4a, 4b and 4c, with consistent spatial patterns across the GrIS. Relatively small differences can be found along the central ice divide and the Southern GrIS. The percentage of nominal density difference with absolute value less than 100 kg/m^3 is 62%, 64% and 64% separately for case 1, 2 and 3. To understand the impact on the nominal densities from the analyzed GRACE gravity solutions, nominal density difference is also separately calculated in three cases listed here.

Case 4: nominal densities in Figure 3a subtracting those in Figure 3b

Case 5: nominal densities in Figure 3a subtracting those in Figure 3c

Case 6: nominal densities in Figure 3b subtracting those in Figure 3c

The nominal density difference in Case 4, 5 and 6 is separately depicted in Figure 5 (d), (e) and (f), with relatively small amplitude shown on the GrIS. The percentage of nominal density difference with absolute value less than 100 kg/m^3 is 95%, 98% and 100% for case 4, 5 and 6, respectively. Therefore, differences in nominal densities shown in Figure 4 can be mainly attributed to the algorithm used to retrieve Envisat data. The impact on the nominal density difference from the analyzed GRACE gravity solutions are relatively small. This suggests that inter-annual mass anomalies separately revealed by CSR, GFZ and JPL published GRACE gravity solutions during 2003-2009 in RL06 are consistent with each other.

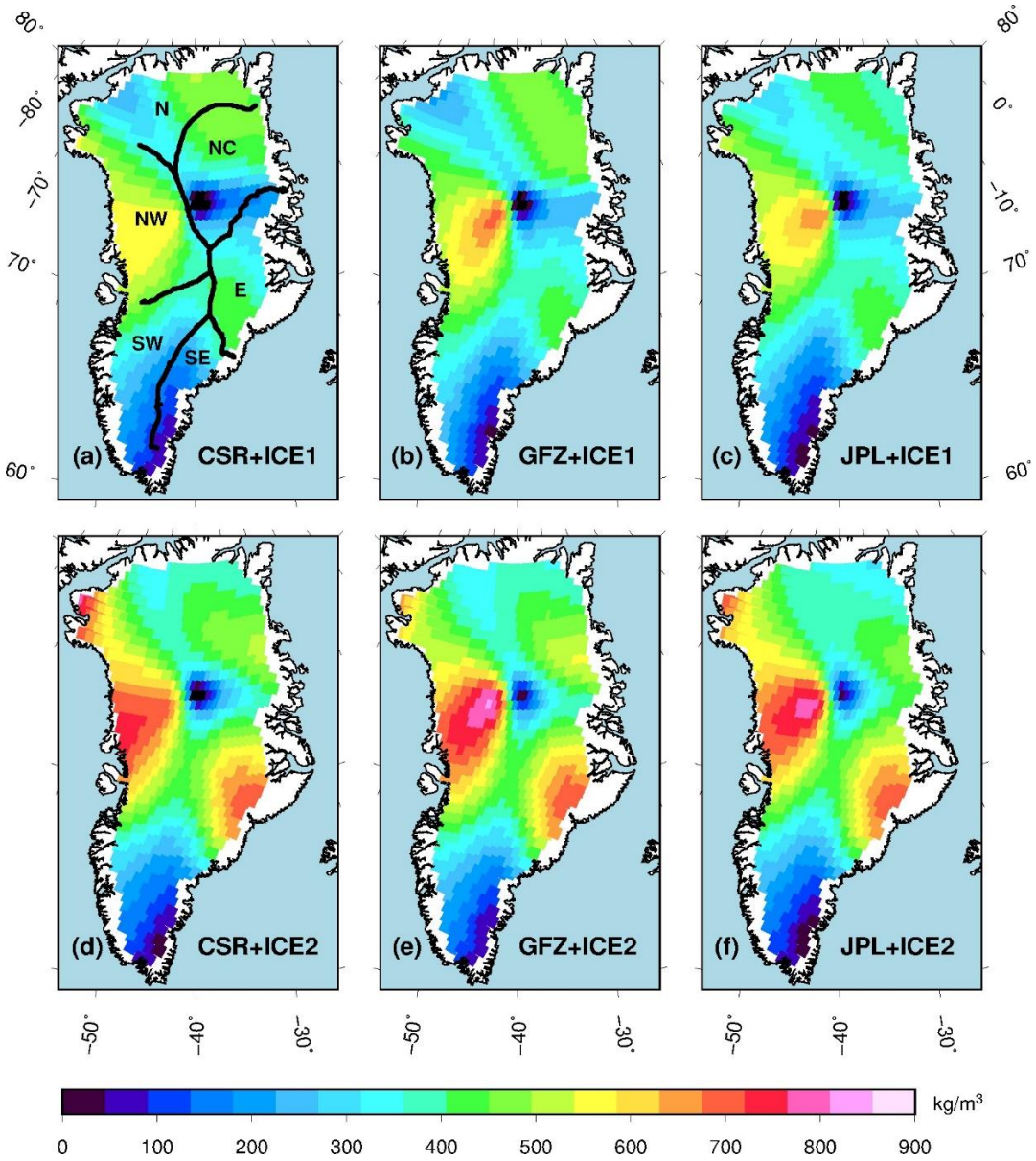

Figure 3 The nominal (average) density of snow/firn inter-annually changing over the GrIS during 2003-2009, based on (a) CSR-published GRACE solutions and Envisat data retrieved by the ICE1 algorithm, abbreviated as CSR+ICE1, (b) GFZ+ICE1, (c) JPL+ICE1, (d) CSR+ICE2, (e) GFZ+ICE2 and (f) JPL+ICE2.

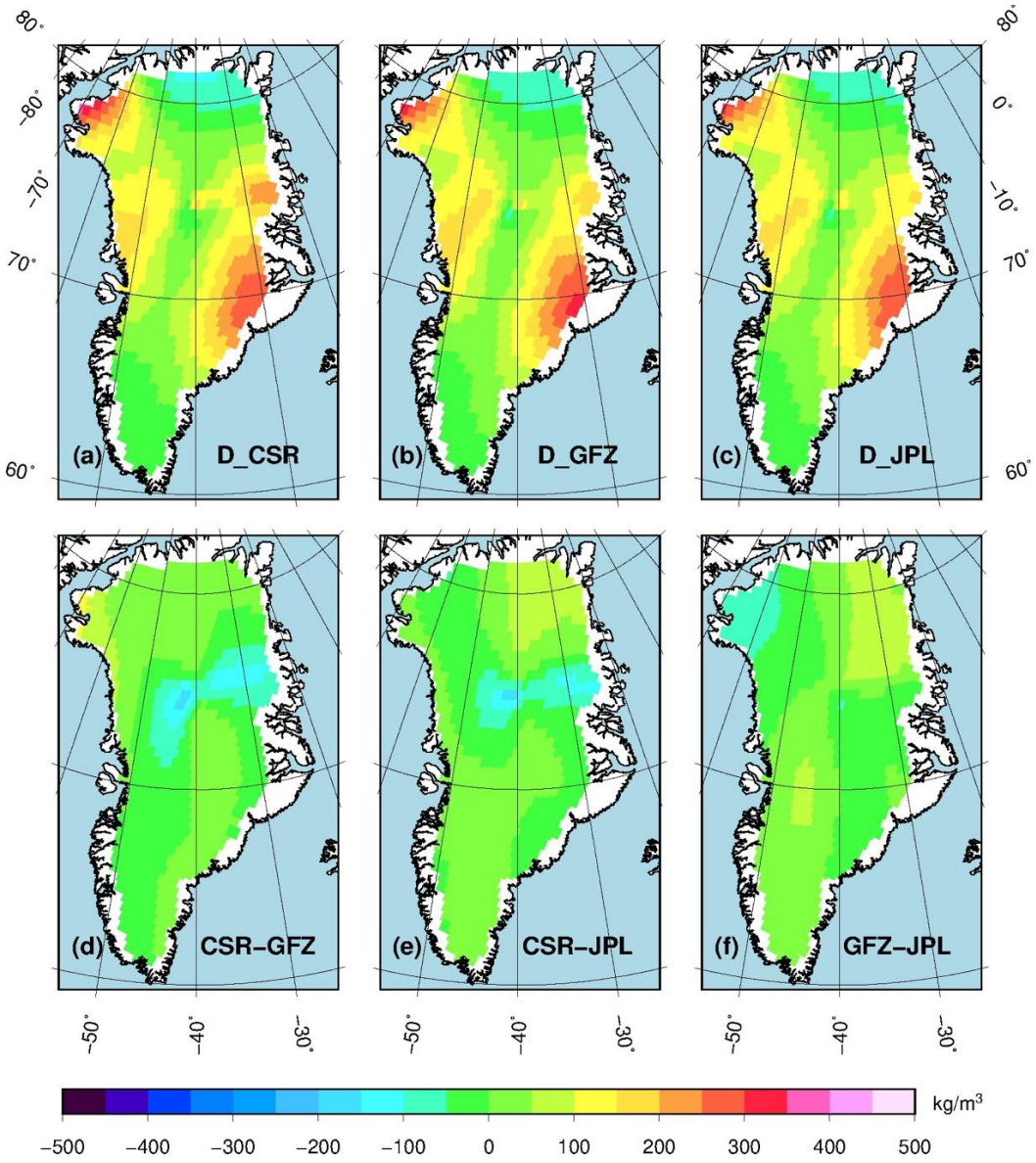

Figure 4 Difference between nominal densities obtained by (a) combining CSR-derived inter-annual mass anomalies separately with the ICE2/ICE1 algorithm retrieved inter-annual elevation anomalies, denoted as D_CSR, (b) D_GFZ, (c) D_JPL, and by (d) combining the ICE1 algorithm retrieved inter-annual elevation anomalies separately with CSR/GFZ derived inter-annual mass anomalies, abbreviated as CSR-GFZ, (e) CSR-JPL, (f) GFZ-JPL over the GrIS.

3.3 Validating satellite-derived density over the GrIS with in situ data

As mentioned in section 2.4, density profiles of 110 ice cores are used to perform the validation after removing the corresponding seasonal variations. Considering that the spatial resolution of GRACE data is about 333 km and that the density profile of a single ice core was measured at a relatively small area, depth-density profiles of 9 ice cores in the Summit Station approximately covering an area of 150 km × 150 km (van der Veen et al., 2001; Montgomery et al., 2018) are first applied to validate satellite-derived density. These 9 ice cores were surveyed in 1987. According to McGrath et al. (2013) and Vandecrux et al. (2017), stable near-

surface firn density was confirmed at Summit Station during the period from the late 1980s to 2010. Therefore, it is reasonable to validate satellite-derived density with these ice cores. The location of these 9 ice cores is provided in Figure S5. The average density of snow/firn with the depth ranging from 0.9 m to 4 m is computed for each ice core at Summit, as shown in Table 2. We then obtain the average density (386±8 kg/m^3) of snow/firn over the Summit Station, based on the densities obtained from these 9 ice cores with depth ranging from 0.9 m to 4 m. To compare this average density value with that from satellite data, we select an area mostly covering the Summit Station (the rectangle in light-blue in Figure S5). Through separately combining one of these three inter-annual mass anomalies from CSR/GFZ/JPL published GRACE solutions with the ICE1-retrieved inter-annual elevation anomalies from Envisat altimetry (GRACE+ICE1), the nominal density of snow/firn is estimated to be 380±26 kg/m^3, 365±33 kg/m^3 and 373±27 kg/m^3, respectively. The corresponding relative errors in absolute value are 2%, 5% and 3%, if the average density (386±8 kg/m^3) from in situ data is regarded as the true value. Similarly, the ICE2-retrieved inter-annual elevation anomalies are also combined separately with these three inter-annual anomalies from CSR/GFZ/JPL published GRACE solutions (GRACE+ICE2) to estimate the nominal density over the same region. The corresponding nominal density is 492±67 kg/m^3, 474±67 kg/m^3 and 483±26 kg/m^3. Apparently, GRACE+ICE2 derived nominal density shows an overestimation of ~100 kg/m^3, compared to the estimates from GRACE+ICE1. That is, over the Summit Station, GRACE+ICE1 derived nominal density agree well with that from ice cores.

Besides, the pattern for average densities from 9 ice cores over Summit Station (column 2 in Table 2) generally follows that average density increases with decreasing latitude (column 3 in Table 2). This tempts us to calculate satellite-derived density at the location of each ice core (column 4~6 in Table 2, and the nominal densities when GRACE is combined with ICE2 are provided in Table S2), although we fully understand that the spatial resolution of satellite data is relatively coarse. Our result illustrates that the above pattern can be generally revealed by satellite-derived densities at all the ice cores, no matter the case GRACE+ICE1 or GRACE+ICE2 is applied. We notice that the mean value of satellite-derived densities at these 9 ice cores is slightly smaller than the corresponding density derived by satellite data at the region (the rectangle in light-blue in Figure S4), with a percentage of 5%~10%. Considering the spatial resolution of satellite data is relatively coarse, we agree that satellite-derived density at the region should be more accurate than that obtained by satellite data at the location of each ice core. We also should realize that satellite-derived density at the location of a single ice core provides meaningful information, especially for the relative density change at different ice cores.

Table 2 Average density obtained at depth of 0.9 m – 4 m at 9 ice cores at Summit Station in 1987, and co-located nominal densities obtained from cases where GRACE is combined with ICE1.

Summit ice cores	Density (0.9 m – 4 m) [kg/m^3]	Latitude [degree]	Satellite-derived density		
			CSR+ICE1	GFZ+ICE1	JPL+ICE 1
Site 15	371	72.9813	314	282	310
Site 13	381	72.8864	337	312	338
Site 37	387	72.6409	332	309	327
Site 31	394	72.3486	380	373	384
Summit	382	72.2939	358	327	348
Site 571	386	72.2120	363	342	356
Site 51	390	71.9266	383	371	380

Site 57	386	71.9205	375	352	366
Site 73	401	71.6022	381	352	369
Area average	386±8	–	358	336	353

In addition, average density calculated from spatially distributed ice core sites is compared with co-located satellite-derived density. Since the accumulation varies with the location of ice cores, here we use the mean of annual accumulation provided by RACMO2/GR to determine the depth used to calculate average density from single ice core, as shown in Figure S5. Totally, density profiles from 110 ice cores are used (the white dots in Figure S5), with the location mostly following the central ice divide in the GrIS. As depicted by Figure 5(a), average densities are relatively large at ice cores close to marginal regions in West GrIS, compared to those in the interior. A similar pattern can be seen from co-located satellite-derived densities, especially from the densities obtained by combining CSR-derived inter-annual mass anomalies and ICE1-retrieved inter-annual elevation anomalies. Nominal densities obtained by combining GFZ/JPL derived inter-annual mass anomalies separately with ICE1/ICE2 retrieved inter-annual elevation anomalies are overestimated at several ice cores close to regions with negative correlation in North Central GrIS. In contrast, at the spots of one ice core over Southwest GrIS and two ice cores over North Central GrIS, satellite-derived density is relatively small, compared to that from the corresponding ice core. The reasons for density underestimation will be further discussed in the next section. To assess the accuracy of nominal densities for the combinations of different GRACE and altimetry products, the scatter plots of nominal density versus the density from in situ data are shown in Figure 6, with the corresponding root mean square error (RMSE) and relative bias (RB) provided in each subplot. For the three cases in GRACE+ICE1, the RMSE of nominal densities is relatively smaller (about 69~81 kg/m^3), compared to those (122~130 kg/m^3) from cases in GRACE+ICE2. A similar pattern can also be found for RB in all the cases. This illustrates that nominal densities derived from GRACE+ICE1 are in better agreement with those from in situ data. We also examine relative error of nominal density derived at each ice core, as depicted by Figure S6. If selecting relative error in absolute value less than 20% as a criterion, the percentage of nominal densities obtained by combining GRACE-derived inter-annual mass anomalies and ICE1-retrieved inter-annual elevation anomalies meeting the criterion is more than 84% (top panel in Figure S6), compared with slightly more than 41% for those obtained by combining GRACE-derived and ICE2-retrieved inter-annual anomalies (bottom panel in Figure S6).

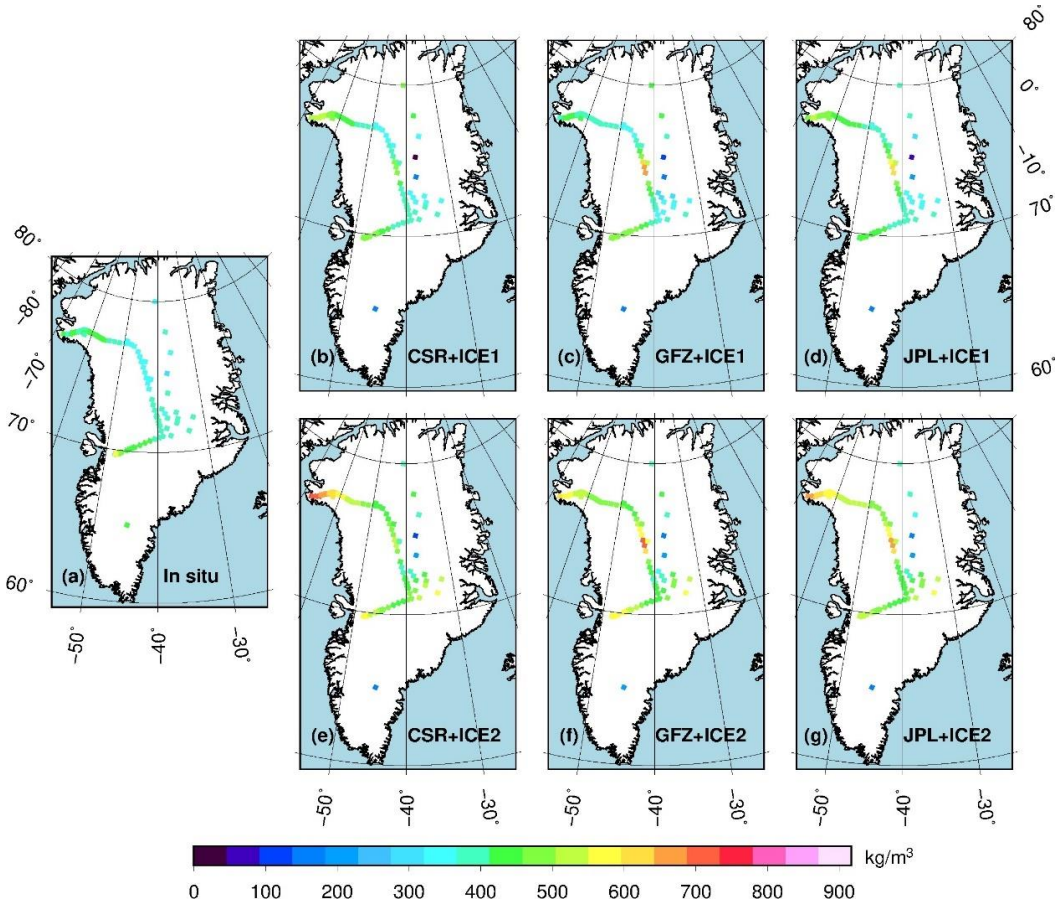

Figure 5 Comparison of (a) average density from 110 ice cores and nominal densities separately estimated from (b) CSR-derived inter-annual mass anomalies and ICE1-retrieved inter-annual elevation anomalies, denoted as CSR+ICE1, (c) GFZ+ICE1, (d) JPL+ICE1, (e) CSR+ICE2, (f) GFZ+ICE2 and (g) JPL+ICE2.

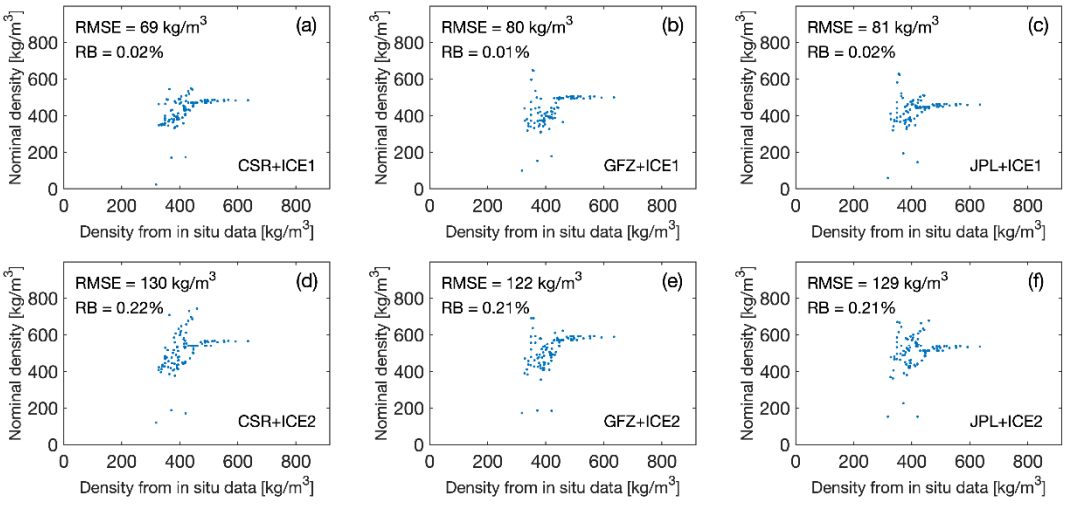

Figure 6 The scatter plots of co-located nominal density derived separately from (a) CSR+ICE1, (b) GFZ+ICE1, (c) JPL+ICE1, (d) CSR+ICE2, (e) GFZ+ICE2, (f) JPL+ICE2, versus the density from in situ data.

4 Discussion

In this study, the improved repeat-track analysis is used to refine Envisat data retrieved separately by the ICE1 and ICE2 algorithms, which enable us to perform the joint analysis of GRACE and Envisat data over the entire GrIS. The results show an improvement in the correlations between the inter-annual mass and elevation anomalies over those of Su et al. (2015), i.e., the percentage of area with correlation coefficient larger than 0.7 increases from 60% to 64%~87% (depending on the algorithm used to retrieve Envisat data), and the percentage of region with negative correlation is reduced from 7% to less than 1%. This can be attributed to the improved repeat-track analysis of Envisat data and the ICE2 algorithm used to retrieve Envisat data. The agreement between inter-annual anomalies from GRACE, Envisat and SMB over most regions, with the exception of parts of Southeast and North Central GrIS, indicates that GRACE gravimetry and Envisat altimetry can detect the same geophysical process captured by SMB from the RACMO2/GR model at the inter-annual timescale. This, to some extent, confirms the correct analysis of GRACE and Envisat data as well as the retrieval of SMB from the RACMO2/GR model.

We attempt to estimate nominal density over the entire GrIS by combining GRACE gravimetry and Envisat altimetry during 2003-2009, with the focus on validating satellite-derived density with that from in situ data for the first time. However, the estimated inter-annually changing nominal density of snow/firn over Southern GrIS is small, compared with those over West GrIS (Figure 3). The comparison with average density value from one ice core in southern Greenland suggests that apparent underestimation of nominal density can be found in Figure 5, with the relative error in absolute value exceeding 50% (Figure S6). As this region is significantly influenced by both mass loss through ice dynamics and mass increase by snow accumulation, it could be associated with the special case we mentioned in Section 2.5. One can consider about a case in which mass was lost through ice dynamics at the inter-annual timescale over the Southern GrIS, while heavy snow accumulation occurred at the same time. In this case, the mass change caused by ice dynamics at the inter-annual scale should be negative over most of the study period. That is, $h_{Ei}^{k} < 0$. As snow was accumulated there so that the corresponding volume change associated with snow accumulation is positive ($h_{Es}^{k} > 0$). Therefore, according to Eq. (3), there could be a situation that the estimated nominal density would be less than the density of snow, if the added volume is larger than the reduced part ($h_{Es}^{k} > \left|h_{Ei}^{k}\right|$). This suggests that the underestimation of the nominal density of snow/firn inter-annually changing over these regions is possible. A future study can be considered to partition the regional mass balance in order to better understand the processes occurring there.

As to weakly positive or negative correlations in the small parts of North Central and Southeast GrIS, we select two regions shown in Figure 2(a) to examine the amplitudes of both inter-annual anomalies and their uncertainties. The root mean square (RMS) of the inter-annual mass/elevation anomalies can be separately calculated for each region. The uncertainty of each inter-annual anomaly is defined like the following: (1) for each month, calculate the average of the inter-annual anomalies from CSR/GFZ/JPL or from the ICE1/ICE2 algorithms, i.e., for July 2003, calculate the average of inter-annual mass anomalies separately from CSR/GFZ/JPL, (2) the uncertainty of the inter-annual anomaly from CSR in July 2003 can be then obtained by the inter-annual anomaly from CSR in July 2003 subtracting the corresponding average value, (3) repeat step (2) for each month and finally generate the time series of uncertainties of inter-annual anomalies from CSR. Thus, the RMS of the time series of uncertainties of inter-annual anomalies

from CSR can be calculated. Similarly, the RMS of uncertainties of inter-annual anomalies from GFZ/JPL/ICE1/ICE2 can be calculated for each region, respectively. As shown in Table S3, the RMS of inter-annual mass anomalies are less than 1 cm in EWH over region 1, and the RMS of inter-annual elevation anomalies are slightly larger than 1 cm in height. Over region 2, the RMS of inter-annual mass/elevation anomalies are 6 times larger than the corresponding value over region 1. Although the RMS of uncertainties of inter-annual mass/elevation anomalies over region 2 is relatively larger than those over region 1, we should admit that the inter-annual anomalies over region 1 could be much easier to be influenced by the uncertainties. Previously, Horwath et al. (2012) found negative correlations between inter-annual anomalies of mass change from GRACE and elevation change from Envisat data over East Antarctica, with the cause attributed to possible systematic errors in the GRACE solutions. In this study, the cause to weakly positive/negative correlations over region 1 may be mainly associated with the small amplitudes of inter-annual signals. As to region 2, the processes including snow accumulation and ice dynamics could be responsible for the weakly positive correlations.

5 Conclusions

The snow/firn density is of fundamental importance in accurately deriving the GrIS mass change from satellite altimetry. In this study, we analyze the inter-annual mass anomalies from the updated GRACE data and elevation anomalies from Envisat altimetry during 2003-2009, aiming at validating satellite-derived density with that from in situ data for the first time. By refining the ICE1/ICE2 retracked elevation change time series through the improved repeat-track analysis, consistent pattern between GRACE-derived and Envisat-observed inter-annual anomalies can be found over most regions in the GrIS. Similar inter-annual variations can also be captured by SMB outputted from the RACMO2/GR model, which suggests that GRACE gravimetry and Envisat altimetry can sense the same geophysical process at the inter-annual timescale over most regions in the GrIS. Assuming that firn compaction associated with air temperature at the inter-annual timescale is small enough and negligible, we attempt to depict the density of snow/firn inter-annually changing over the whole GrIS by purely using satellite data. Our results show that the nominal density of snow/firn is relatively large over the West GrIS, and relatively small nominal densities appear over Southern GrIS. By comparing the estimated nominal densities in 6 cases, the impact on the nominal density from the algorithm used to retrieved Envisat data is more significant than that from GRACE gravity solutions published by the three data analysis centers (CSR/GFZ/JPL).

Finally, satellite-derived densities are validated with those provided by in situ data from 110 ice cores over the GrIS after removing firn layers dominated by seasonal variations. On the one hand, over Central GrIS (at the regional scale), density profiles from 9 ice cores covering a region of $150\ \text{km} \times 150\ \text{km}$ are used to examine satellite-derived density there. GRACE+ICE1 obtained density agrees well with that from these ice cores, with the relative error less than 5%. GRACE+ICE2 derived density shows an overestimation, with a magnitude of 100 kg/m3. On the other hand, satellite-derived density is compared with that from each ice core. By calculating RMSE, RB and relative error, nominal densities obtained by GRACE+ICE1 rather than GRACE+ICE2 show better agreement with those from in situ data. To some extent, this confirms that the nominal density of snow/firn inter-annually changing over the GrIS obtained by combining GRACE gravimetry and Envisat altimetry can be largely explained by the inter-annual variations in upper firn layer density. Geodetic observations of mass change with higher

561 spatial resolution and elevation change covering a longer time span in future may contribute to
562 better constraining the snow/firn density of polar ice sheets.

563 **Acknowledgments**

564 This research is primarily supported by the National Natural Science Foundation of China (Grant
565 No. 41804014, 41931074), the National Key R&D Program of China (Grant No.
566 2018YFC1503503), and the Strategic Priority Research Program of the Chinese Academy of
567 Sciences (Grant No. XDA19070302), and by the U.S. National Science Foundation via the
568 Belmont Forum/IGFA Grant (ICER-1342644). Chungyen Kuo is partially supported by National
569 Cheng Kung University, Taiwan. GRACE data products are from NASA via CSR, GFZ and JPL,
570 which can be assessed at http://podaac.jpl.nasa.gov/grace and http://isdc.gfz-potsdam.de/grace.
571 Envisat altimetry GDR data are from ESA/ESRIN through ra2-ftp-ds.eo.esa.int. Profiles of
572 snow/firn density can be assessed at the Arctic Data Center (https://arcticdata.io). Some figures
573 in the paper are generated by using Generic Mapping Tool (GMT) (Wessel and Smith, 1991).
574 We thank Prof. van den Broeke for providing SMB data from the RACMO2/GR model.

575 **References**

576 Alley, R.B., Meese, D., Shuman, C.A., Gow, A.J., Taylor, K.C., Ram, M., Waddington, E.D.,
577 Mayewski, P.A., & Zielinski, G.A. (1993), Abrupt increase in Greenland snow accumulation at
578 the end of the Younger Dryas event, Nature, 362, 527-528.

579 Arthern, R.J., & Wingham, D.J. (1998), The natural fluctuations of firn densification and their
580 effect on the geodetic determination of ice sheet mass balance, Clim. Change, 40(3-4), 605-624.

581 Bader, H. (1953), Sorge's law of densification of snow on high polar glaciers, J. Glaciol., 319-
582 322.

583 Bamber, J. L. (1994), Ice sheet altimeter processing scheme, Int. J. Remote Sens., 15, 925-938.

584 Bamber, J.L., Westaway, R.M., Marzeion, B., & Wouters, B. (2018), The land ice contribution to
585 sea level during the satellite era, Environ. Res. Lett., 13, 063008.

586 Bettadpur, S. (2018), UTCSR Level-2 Processing Standards Document For Level-2 Product
587 Release 0006, Technical Report GRACE, 327-742.

588 Bolch, T., Sorensen, L.S., Simonsen, S.B., Molg, N., Machguth, H., Rastner, P., & Paul, F.
589 (2013), Mass loss of Greenland's glaciers and ice caps 2003-2008 revealed from ICESat laser
590 altimetry data, Geophys. Res. Lett., 40, 875-881. doi:10.1002/grl.50270

591 Bolzan, J.F., & Strobel, M. (1994), Accumulation-rate variations around Summit, Greenland, J.
592 Glaciol., 40(134), 56-66.

593 Dahle, C., Flechtner, F., Murböck, M., Michalak, G., Neumayer, H., Abrykosov, O., Reinhold,
594 A., & König, R. (2018), GRACE Geopotential GSM Coefficients GFZ RL06. V. 6.0. GFZ Data
595 Services. http://doi.org/10.5880/GFZ.GRACE_06_GSM.

596 Dibb, J.E., & Fahnestock, M. (2004), Snow accumulation, surface height change, and firn
597 densification at Summit, Greenland: Insights from 2 years of in situ observation, J. Geophys.
598 Res., 109, D24113.

599 Ewert, H., Groh, A., & Dietrich, R. (2012), Volume and mass changes of the Greenland ice sheet
600 inferred from ICESat and GRACE, J. Geodyn. 59-60, 111-123.

601 Fausto, R.S., Box, J.E., Vandecrux, B., van As, D., Steffen, K., MacFerrin, M.J., Machguth, H.,
602 Colgan, W., Koenig, L.S., McGrath, D., Charalampidis, C., & Braithwaite, R. J. (2018), A snow
603 density dataset for improving surface boundary conditions in Greenland ice sheet firn modeling,
604 Front. Earth Sci.,6:51, doi:10.3389/feart.2018.00051.

605 Fettweis, X., Box, J.E., Agosta, C., Amory, C., Kittel, C., Lang, C., van As, D., Machguth, H., &
606 Gallee, H. (2017), Reconstructions of the 1900-2015 Greenland ice sheet surface mass balance
607 using the regional climate MAR model, The Cryosphere, 11, 1015-1033.

608 Graeter, K.A., Osterberg, E.C., Ferris, D.G., Hawley, R.L., Marshall, H.P., Lewis, G., Meehan,
609 T., McCarthy, F., Overly, T., & Birkel, S.D. (2017), Ice core records of West Greenland melt and
610 climate forcing, Geophys. Res. Lett., 45, 3164-3172.

611 Groh, A., Horwath, M., Horvath, A., Meister, R., Sørensen, L.S., Barletta, V.R., Forsberg, R.,
612 Wouters, B., Ditmar, P., Ran, J., Klees, R., Su, X., Shang, K., Guo, J., Shum, C.K., Schrama, E.,
613 & Shepherd, A. (2019), Evaluating GRACE Mass Change Time Series for the Antarctic and
614 Greenland Ice Sheet—Methods and Results, Geosciences, 9, 415.
615 doi:10.3390/geosciences9100415.

616 Guo, J.Y., Duan, X.J., & Shum, C.K. (2010), Non-isotropic Gaussian smoothing and leakage
617 reduction for determining mass changes over land and ocean using GRACE data, Geophys. J.
618 Int., 181(1), 290-302.

619 Guo, J.Y., Huang, Z.W., Shum, C.K., & van der Wal, W. (2012), Comparisons among
620 contemporary glacial isostatic adjustment models, J. Geodyn., 61, 129-137.

621 Howat, I.M., Smith, B.E., Joughin, I., & Scambos, T.A. (2008), Rates of southeast Greenland ice
622 volume loss from combined ICESat and ASTER observations, Geophys. Res. Lett., 35, L17505,
623 doi:10.1029/2008GL034496.

624 Horwath, M., Legresy, B., Remy, F., Blarel, F., & Lemoine, J.M. (2012), Consistent patterns of
625 Antarctic ice sheet inter-annual variations from ENVISAT radar altimetry and GRACE satellite
626 gravimetry, Geophys. J. Int., 189(2), 863-876.

627 Montgomery, L., Koenig, L., & Alexander, P. (2018), The SUMup dataset: compiled
628 measurements of surface mass balance components over ice sheets and sea ice with analysis over
629 Greenland, Earth System Science Data, 10, 1959-1985, doi: 10.5194/essd-10-1959-2018.Krabill,
630 W., R. Thomas, K. Jezek, K. Kuivinen, and S. Manizade (1995), Greenland ice sheet thickness
631 changes measured by laser altimetry, Geophys. Res. Lett., 22(17), 2341-2344.

632 Kuipers Munneke, P., Ligtenberg, S.R.M., Noel, B.P.Y., Howat, I.M., Box, J.E., Mosley-
633 Thomposon, E., McConnell, J.R., Steffen, K., Harper, J.T., Das, S.B., & van den Broeke, M.R.
634 (2015), Elevation change of the Greenland ice sheet due to surface mass balance and firn
635 processes, 1960-2014, Cryosphere, 9, 2009-2025. doi:10.5194/tx-9-2009-2015

636 Legresy, B., & Remy, F. (1997), Surface characteristics of the Antarctic ice sheet and altimetric
637 observations, J. Glaciol., 43(144), 265-275.

638 Li, J., & Zwally, H.J. (2011), Modeling of firn compaction for estimating ice-sheet mass change
639 from observed ice-sheet elevation change, Annals of Glaciology, 52(59), 1-7.

640 McMillan, M., Leeson, A., Shepherd, A., Briggs, K., Armitage, T.W.K., Hogg, A., Kuipers
641 Munneke, P., van den Broeke, M., Noel, B., van de Berg, W.J., Ligtenberg, S., Horwath, M.,

642 Groh, A., Muir, A., & Gilbert, L. (2016), A high-resolution record of Greenland mass balance,
643 Geophys. Res. Lett., 43, 7002-7010.

644 Montgomery, L., Koenig, L., & Alexander, P. (2018), The SUMup dataset: compiled
645 measurements of surface mass balance components over ice sheets and sea ice with analysis over
646 Greenland, Earth System Science Data, 10, 1959-1985, doi: 10.5194/essd-10-1959-2018.

647 Nilsson, J., Gardner, A., Sorensen, L.S., & Forsberg, R. (2016), Improved retrieval of land ice
648 topography from CryoSat-2 data and its impact for volume-change estimation of the Greenland
649 ice sheet, Cryosphere, 10, 2953-2969.

650 Noel, B., van de Berg, W.J., van Wessem, J.M., van Meijgaard, E., van As, D., Lenaerts, J.T.M.,
651 Lhermitte, S., Kuipers Munneke, P., Paul Smeets, C.J.P., van Ulft, L.H., van de Wal, R.S.W., &
652 van den Broeke, M.R. (2018), Modelling the climate and surface mass balance of polar ice sheets
653 using RACMO2 – Part 1: Greenland (1958-2016), The Cryosphere, 12, 811-831.

654 Sasgen, I., van den Broeke, M., Bamber, J.L., Rignot, E., Sorensen, L.S., Wouters, B., Martinec,
655 Z., Velicogna, I., & Simonsen, S.B. (2012), Time and origin of recent regional ice-mass loss in
656 Greenland, Earth Planet. Sci. Lett., 333-334, 293-303.

657 Shepherd, A., Ivins, E.R., A, G., Barletta, V.R., Bentley, M.J., Bettadpur, S., Briggs, K.H.,
658 Bromwich, D.H., Forsberg, R., Galin, N., Horwath, M., Jacobs, S., Joughin, I., King, M.A.,
659 Lenaerts, J.T.M., Li, J., Ligtenberg, S.R.M., Luckman, A., Luthcke, S.B., McMillan, M.,
660 Meister, R., Milne, G., Mouginot, J., Muir, A., Nicolas, J.P., Paden, J., Payne, A.J., Pritchard,
661 H., Rignot, E., Rott, H., Sorensen, L.S., Scambos, T.A., Scheuchl, B., Schrama, E.J.O., Smith,
662 B., Sundal, A.V., van Angelen, J.H., van de Berg, W.J., van den Broeke, M.R., Vaughan, D.G.,
663 Velicogna, I., Wahr, J., Whitehouse, P.L., Wingham, D.J., Yi, D., Young, D., & Zwally, H.J.
664 (2012), A reconciled estimate of ice-sheet mass balance, Science, 338, 1183-1189.

665 Slobbe, D.C., Ditmar, P., & Lindenbergh, R.C. (2009), Estimating the rates of mass change, ice
666 volume change and snow volume change in Greenland from ICESat and GRACE data, Geophys,
667 J. Int., 176, 95-106.

668 Sorensen, L.S., Simonsen, S.B., Nielsen, K., Lucas-Picher, P., Spada, G., Adalgeirsdottir, G.,
669 Forsberg, R., & Hvidberg, C.S. (2011), Mass balance of the Greenland ice sheet (2003-2008)
670 from ICESat data – the impact of interpolation, sampling and firn density, Cryosphere, 5, 173-
671 186.

672 Sorensen, L.S., Simonsen, S.B., Meister, R., Forsberg, R., Levinsen, J.F., & Flament, T. (2015),
673 Envisat-derived elevation changes of the Greenland ice sheet, and a comparison with ICESat
674 results in the accumulation area, Remote Sens. Environ., 160, 56-62.

675 Steger, C.R., Reijmer, C.H., van den Broeke, M.R., Wever, N., Forster, R.R., Koenig, L.S.,
676 Kuipers Munneke, P., Lehning, M., Lhermitte, S., Ligtenberg, S.R.M., Miege, C., & Noel,
677 B.P.Y. (2017), Firn meltwater retention on the Greenland ice sheet: a model comparison, Front.
678 Earth Sci. 5:3, doi:10.3389/feart.2017.00003.

679 Su, X., Shum, C.K., Guo, J., Duan, J., Howat, I., & Y., Yi (2015), High resolution Greenland ice
680 sheet inter-annual mass variations combining GRACE gravimetry and Envisat altimetry, Earth
681 Planet. Sci. Lett., 422, 11-17.

682 Su, X., Shum, C.K., Kuo, Chungyen, & Yi, Y. (2016), Improved Envisat altimetry ice sheet
683 elevation change data processing algorithms using repeat-track analysis, IEEE Geosci. Remote
684 S., 13(8), 1099-1103. doi:10.1109/LGRS.2016.2567486

685 Sun, Y., Riva, R., & Ditmar, P. (2016), Optimizing estimates of annual variations and trends in
686 geocenter motion and J2 from a combination of GRACE data and geophysical models, J.
687 Geophys. Res. Solid Earth, 121, doi:10.1002/2016JB013073.

688 Sutterley, T.C., Velicogna, I., Csatho, B., van den Broeke, M., Rezvan-Behbahani, S., &
689 Babonis, G. (2014), Evaluating Greenland glacial isostatic adjustment corrections using GRACE,
690 altimetry and surface mass balance data, Environ. Res. Lett., 9, 1-9. doi:10.1088/1748-
691 9326/g/1/014004

692 Swenson, S., Chambers, D., & Wahr, J. (2008), Estimating geocenter variations from a
693 combination of GRACE and ocean model output, J. Geophys. Res., 113, B08410,
694 doi:10.1029/2007JB005338

695 Tapley, B.D., Bettadpur, S., Watkins, M., & Reigber, C. (2004), The gravity recovery and
696 climate experiment: Mission overview and early results, Geophys. Res. Lett., 31, L09607,
697 doi:10.1029/2004GL019920

698 Thomas, R., Csatho, B., Davis, C., Kim, C., Krabill, W., Manizade, S., McConnell, J., &
699 Sonntag, J. (2001), Mass balance of higher-elevation parts of the Greenland ice sheet, J.
700 Geophys. Res., 106(D24), 33,707-33,716.

701 Thomas, R., Frederick, E., Krabill, W., Manizade, S., & Martin, C. (2006), Progressive increase
702 in ice loss from Greenland, Geophys. Res. Lett., 33, L10503.

703 van den Broeke, Bamber, J., Ettema, J., Rignot, E., Schrama, E., van den Berg, W.J., van
704 Meijgaard, E., Velicogna, I., & Wouters, B. (2009), Partitioning recent Greenland mass loss,
705 Science, 326, 984-986.

706 Wahr, J., Wingham, D., & Bentley, C. (2000). A method of combining ICESat and GRACE
707 satellite data to constrain Antarctic mass balance, J. Geophys. Res., 105(B7), 16279-16294.

708 Wessel, P., & Smith, W.H.F. (1991), Free software helps map and display data, Eos Trans. AGU,
709 72(41), 441. doi:10.1029/90EO00319

710 Wingham, D.J., Rapley, C.G., & Griffiths, H.D. (1986). New techniques in satellite altimeter
711 tracking systems, Proceedings of the IGARSS Symposium, Zurich, 8-11 September, edited by
712 T.D. Guyenne and J.J. Hunt (European Space Agency), SP-254, pp. 1339-1344.

713 Wouters, B., Bamber, J.L., van den Broeke, M.R., Lenaerts, J.T.M., & Sasgen, I. (2013), Limits
714 in detecting acceleration of ice sheet mass loss due to climate variability, Nature Geosci., 6, 613-
715 616. doi:10.1038/NGEO1874

716 Yuan, D.-N. (2018), JPL Level-2 Processing Standards Document For Level-2 Product Release
717 06, Jet Propulsion Laboratory, California Institute of Technology, June 2018. GRACE 327-744.

718 Zwally, H.J., Brenner, A.C., Major, J.A., Bindschadler, R.A., & Marsh, J.G. (1989), Growth of
719 Greenland ice sheet: measurement, Science, 246, 1587-1589.

720 Zwally, H.J., & Li, J. (2002), Seasonal and inter-annual variations of firn densification and ice-
721 sheet surface elevation at the Greenland summit, J. Glaciol., 48(161), 199-207.

722 Zwally, H.J., Giovinetto, M.B., Li, J., Cornejo, H.G., Beckley, M.A., Brenner, A. C., Saba, J.L.,
723 & Yi, D. (2005), Mass changes of the Greenland and Antarctic ice sheets and shelves and
724 contributions to sea-level rise: 1992-2002, J. Glaciol., 51(175), 509-527.